

Titan's Obliquity as evidence for a subsurface ocean?

Rose-Marie Baland , Tim Van Hoolst, Marie Yseboodt and Ö. Karatekin
Royal Observatory of Belgium, Brussels, Belgium
 Email: balandrm@oma.be

April 2011

The final version of this preprint is published in Astronomy & Astrophysics
 DOI: 10.1051/0004-6361/201116578

Abstract

On the basis of gravity and radar observations with the Cassini spacecraft, the moment of inertia of Titan and the orientation of Titan's rotation axis have been estimated in recent studies. According to the observed orientation, Titan is close to the Cassini state. However, the observed obliquity is inconsistent with the estimate of the moment of inertia for an entirely solid Titan occupying the Cassini state. We propose a new Cassini state model for Titan in which we assume the presence of a liquid water ocean beneath an ice shell and consider the gravitational and pressure torques arising between the different layers of the satellite. With the new model, we find a closer agreement between the moment of inertia and the rotation state than for the solid case, strengthening the possibility that Titan has a subsurface ocean.

1 Introduction

On the basis of Cassini radar images, [6] and [7] precisely measured the orientation of the rotation axis of Titan. Using the orientation of the normal to the orbit of Titan given in the IAU recommendations (Seidelmann et al. 2007), they determined the obliquity to be about 0.3° . They also showed that the rotation axis makes a small angle of about 0.1° with respect to the plane defined by the normal to the Laplace plane and the normal to the orbit and, as a result, they stated that Titan is close to the Cassini state.

From Cassini radio tracking, the quadrupole field of Titan has been found to be consistent with a body in hydrostatic equilibrium with a moment of inertia $C/MR^2 = 0.3414 \pm 0.0005$ [4]. However, in a study of the Cassini state generalized to a multi-frequency orbital node precession in which Titan was considered as an entirely solid body, [2] found that the 0.3° obliquity implies a moment of inertia of $C = 0.55MR^2$, which is not only inconsistent with the above hydrostatic value of the moment of inertia but would also imply a physically implausible interior structure with higher mass density towards the surface than towards the center. In their conclusion, the authors proposed that a liquid ocean could partially decouple the shell from the interior.

The obliquity of the Cassini sate, which is an equilibrium orientation of the rotation axis of a synchronous satellite, can be derived from angular momentum equations in much the same way

TABLE 1 – **Orbital theory of Titan and solid Cassini state** : columns 2 to 5 : Amplitudes, frequencies, periods, and phases of the orbit precession adapted from [11]. They give the orbital precession in the equatorial plane of Saturn and used J1980 as the time origin. Here we consider the Laplace plane and J2000 time origin. The Laplace plane has a node of 184.578° and an inclination (also called tilt) of 0.6420° with respect to the equatorial plane of Saturn. Since the tilt is small, the frequency and amplitude of the orbital precession are almost the same with respect to the Laplace plane as to the equatorial plane of Saturn. The x-axis of the Laplace plane is taken as the node of the Laplace plane on the equatorial plane of Saturn. The obliquity amplitudes and resonance factors (fr_j) of the solid Cassini state model presented in Section 3 are given in the last two columns.

j	i_j (deg)	$\dot{\Omega}_j$ (rad/year)	period (years)	γ_j (deg)	ε_j (deg)	fr_j
1	0.3197	-0.00893124	-703.51	160.691	0.1199	1.38
2	0.0150	-0.00192554	-3263.07	102.230	0.0009	1.06
3	0.0129	0.42659824	14.73	292.867	-0.0120	–
4	0.0022	-0.21329912	-29.46	222.920	-0.0026	1.18

as for the periodic variations about its equilibrium rotation rate, but with different assumptions concerning the timescales involved (long timescales for the obliquity and short timescales for the length-of-day variations). The influence of a global liquid layer on the LOD variations of Titan and on the librations of the Galilean satellites was investigated in [9] and [1], respectively. Here, we extend their method, considering the appropriate timescales, to the Cassini state. By considering the gravitational and pressure torques between the different layers of the satellite, we show that the orientation of the rotation axis given in [6] can be partially reconciled with the moment of inertia given in [4].

2 The Cassini state for a solid Titan

In the classical Cassini state, the rotation axis, the normal to the orbit, and the normal to the Laplace plane of a synchronous solid satellite remain in the same plane since the rotation axis has the same constant precession rate as the normal to the orbit about the normal to the Laplace plane, which is, by definition, the mean orbital plane of the satellite. The obliquity is then the constant angle between the rotation axis and the normal to the orbit.

To be able to develop the Cassini state in the presence of a liquid subsurface ocean, we first present the generalization of the Cassini state of a solid Titan to a multi-frequency node precession, following [3]. Neglecting wobble, the rotation axis coincides with the principal axis of the polar moment of inertia C and the angular momentum equation is

$$\begin{aligned}
 n_T C \frac{d\hat{s}}{dt} &= n_T \kappa (\hat{s} \wedge \hat{n}), \\
 \kappa &= \frac{3}{2} MR^2 (-C_{20} + 2C_{22}) n_T = \frac{3}{2} (C - A) n_T,
 \end{aligned}
 \tag{1}$$

where $\hat{s} = (s_x, s_y, s_z)$ and $\hat{n} = (n_x, n_y, n_z)$ are the unit vectors along the rotation axis and the normal to the orbit, expressed in coordinates (x, y) of the Laplace plane and z along the normal. In addition, M and R are the mass and mean radius, C_{20} and C_{22} are the second-degree gravity field

coefficients, A is the smallest moment of inertia, and n_T is the mean motion, equal to the rotation rate, of Titan. The right-hand member is the gravitational torque (averaged over the orbital period) exerted by Saturn. The vectorial equation is then projected on the Laplace plane, where the motions of the projected rotation axis and orbit normal are easy to parametrize

$$\frac{dS}{dt} = I \frac{\kappa}{C} (N - S) \quad (2)$$

with $S = s_x + Is_y$ and $N = n_x + In_y$, $I = \sqrt{-1}$. Equation (2) is correct up to the first order in small obliquity, eccentricity and inclination (see Eq. (46) of [3] in which a sign has been corrected). We first assume that the orbital precession N , which causes the rotation axis precession, is zero in order to get the free spin precession mode whose frequency ω_f depends only on the physical properties of the satellite

$$\omega_f = \frac{\kappa}{C}. \quad (3)$$

To compute the forced solution, the orbital precession is written as a series expansion

$$N = \sum_j \sin i_j e^{I(\dot{\Omega}_j t + \gamma_j - \pi/2)}, \quad (4)$$

where the inclination amplitudes i_j , frequencies $\dot{\Omega}_j$, and phases γ_j associated with the node precession of the orbit with respect to the Laplace plane have been taken, up to $j = 4$, from [11] and are given in Table 1. The parameters $\dot{\Omega}_1$ and i_1 are the main precession rate (with a period of 703.51 years) and the small mean inclination (0.3197°) of the orbital plane, considered in the classical Cassini state. The forced solution of Eq.(2) is then

$$S = \sum_j \sin (i_j + \varepsilon_j) e^{I(\dot{\Omega}_j t + \gamma_j - \pi/2)}, \quad (5)$$

where, correct up to the first order in ε_j and i_j , the obliquity amplitude ε_j associated with the frequency $\dot{\Omega}_j$ is given by

$$\varepsilon_j = -\frac{i_j \dot{\Omega}_j}{(\omega_f + \dot{\Omega}_j)}. \quad (6)$$

The obliquity ε at any time is the non-constant angle between the rotation axis and the normal to the orbit and oscillates between two extreme values ε_{min} and ε_{max} such that

$$\varepsilon \cong \sin \varepsilon = \|S - N\| \quad (7)$$

$$\varepsilon_{min} = 2 \max_j \{|\varepsilon_j|\} - \sum_j |\varepsilon_j| \leq \varepsilon \leq \sum_j |\varepsilon_j| = \varepsilon_{max}. \quad (8)$$

In this generalization, the normal to the Laplace plane, the normal to the orbit, and the rotation axis are not coplanar and the small angular deviation δ of the spin axis with respect to the plane defined by the other axes is

$$\delta \cong \sin \delta = (n_x s_y - n_y s_x) / \|N\|. \quad (9)$$

Since the frequency ω_f is positive, $\omega_f + \dot{\Omega}_j$ can be close to zero if $\dot{\Omega}_j < 0$, and the coefficient ε_j can be amplified by a resonance. For $\dot{\Omega}_j < 0$, we define ‘‘resonance factors’’, fr_j , which describe the amplification of ε_j caused by the resonance and are close to one far from resonance, given by

$$fr_j = \max(|\omega_f|, |\dot{\Omega}_j|)/|\omega_f + \dot{\Omega}_j| \quad (10)$$

For $C_{20} = -31.808 \times 10^{-6}$, $C_{22} = 9.983 \times 10^{-6}$, and $C = 0.3414MR^2$ (Iess et al. 2010), the resonant factors fr_j are close to one because the free mode period is 191.91 years. Therefore, no significant resonant amplification (see Table 1) occurs and the obliquity variations are small. The obliquity ε of about 0.12° , and the maximal deviation δ of about 0.02° (Fig. 4) are inconsistent with the results of [6].

3 Titan with a liquid ocean

3.1 A new Cassini state solution

We now assume that Titan consists of four homogeneous layers : an ice shell (*sh*), a liquid ocean (*o*), an ice mantle (*m*), and an ice/rock core (*c*). The solid layer composed of the mantle and the core is also called interior (*in*) hereafter. The shell and the interior are considered to behave rigidly. For the solid layers, the angular momentum vector \vec{H}_l can be written as the product of the polar moment of inertia C_l and the rotation vector $n_T \hat{s}_l$. The angular momentum equations take the form

$$n_T C_{sh} \frac{d\hat{s}_{sh}}{dt} = \vec{\Gamma}_{sh,ext} + \vec{\Gamma}_{sh,ext}^p + \vec{\Gamma}_{sh,int} + \vec{\Gamma}_{sh,int}^p, \quad (11)$$

$$\frac{d\vec{H}_o}{dt} = \vec{\Gamma}_{o,ext} + \vec{\Gamma}_{o,ext}^p + \vec{\Gamma}_{o,int} + \vec{\Gamma}_{o,int}^p, \quad (12)$$

$$n_T C_{in} \frac{d\hat{s}_{in}}{dt} = \vec{\Gamma}_{in,ext} + \vec{\Gamma}_{in,ext}^p + \vec{\Gamma}_{in,int} + \vec{\Gamma}_{in,int}^p, \quad (13)$$

where the external gravitational torque exerted by Saturn on layer (*l*), $\vec{\Gamma}_{l,ext}$, is equal to $-\int_{V_l} (\vec{r} \wedge \rho_j \nabla W) dV$, where W is the gravitational potential of Saturn averaged over the orbital period, \vec{r} is the position vector of the points located inside the volume V_l of layer (*l*), and $\vec{\Gamma}_{l,int}$ is the internal gravitational torque due to layers with a different orientation than layer (*l*). The liquid ocean induces pressure torques at the interfaces between the solid layers and the ocean. As we shall see later, the pressure torques can be interpreted as a modification of the external and internal gravitational torques and are therefore denoted by $\vec{\Gamma}_{l,ext}^p$ and $\vec{\Gamma}_{l,int}^p$.

The external gravitational torques on the shell and the interior are written as in Eq.(1) for the solid case

$$\vec{\Gamma}_{sh,ext} = n_T \kappa_{sh} (\hat{s}_{sh} \wedge \hat{n}), \text{ with } \kappa_{sh} = \frac{3}{2} (C_{sh} - A_{sh}) n_T, \quad (14)$$

$$\vec{\Gamma}_{in,ext} = n_T \kappa_{in} (\hat{s}_{in} \wedge \hat{n}), \text{ with } \kappa_{in} = \frac{3}{2} (C_{in} - A_{in}) n_T. \quad (15)$$

We divide the ocean into a top part and a bottom part, respectively, above and below an arbitrary chosen sphere inside the ocean. The pole axes of the top and bottom parts are those of the shell and the interior, respectively, and

$$\begin{aligned} \vec{\Gamma}_{o,ext} &= n_T \kappa_{o,t} (\hat{s}_{sh} \wedge \hat{n}) + n_T \kappa_{o,b} (\hat{s}_{in} \wedge \hat{n}), \\ \kappa_{o,t} &= \frac{3}{2} (C_{o,t} - A_{o,t}) n_T, \quad \kappa_{o,b} = \frac{3}{2} (C_{o,b} - A_{o,b}) n_T, \end{aligned} \quad (16)$$

where $(C_{o,t} - A_{o,t})$ and $(C_{o,b} - A_{o,b})$ are the moment of inertia difference of the top and bottom part, respectively. For the long timescales considered here, it is a very good approximation to assume that the fluid is in hydrostatic equilibrium, therefore W induces a pressure P_{ext} in the ocean such that $\nabla P_{ext} = -\rho_o \nabla W$. The modification of the external torque on the interior because of the pressure is, applying Gauss' theorem,

$$\vec{\Gamma}_{in,ext}^p = \int_{V_{in}} (\vec{r} \wedge \rho_o \nabla W) dV, \quad (17)$$

where \vec{r} is the position vector of the points located inside the volume V_{in} of the interior. It then follows that

$$\vec{\Gamma}_{in,ext}^p = n_T \kappa_{o,b} (\hat{s}_{in} \wedge \hat{n}). \quad (18)$$

In the same way, the modification of the external torques on both the shell and the ocean because of the pressure effect are

$$\vec{\Gamma}_{sh,ext}^p = n_T \kappa_{o,t} (\hat{s}_{sh} \wedge \hat{n}), \quad (19)$$

$$\vec{\Gamma}_{o,ext}^p = -n_T \kappa_{o,b} (\hat{s}_{in} \wedge \hat{n}) - n_T \kappa_{o,t} (\hat{s}_{sh} \wedge \hat{n}). \quad (20)$$

By using Eq. (16), we see that $\vec{\Gamma}_{o,ext}^p + \vec{\Gamma}_{o,ext}^p = 0$, which is a consequence of hydrostatic equilibrium.

Two layers with different obliquities and coincident axes of the moment of inertia B (on average, as a consequence of the Cassini state) exert a gravitational torque on each other tending to align their pole axis with each other. This internal gravitational torque on any layer (l) is given by

$$\vec{\Gamma}_{l,int} = - \int_{V_l} (\vec{r} \wedge \rho_l \nabla \Phi) dV, \quad (21)$$

where Φ is the internal gravitational potential, averaged over the orbital period, of the layers with a different obliquity than layer (l). From [8], we express the torque on the interior due to the shell and the top ocean and the torque on the shell caused by the misalignment with the bottom ocean and the interior as

$$\vec{\Gamma}_{in,int} = -(8\pi G/5)(C_{in} - A_{in}) [\rho_{sh}(\alpha_{sh} - \alpha_o + \beta_{sh}/2 - \beta_o/2) + \rho_o(\alpha_o + \beta_o/2)] (\hat{s}_{sh} \wedge \hat{s}_{in}), \quad (22)$$

$$\vec{\Gamma}_{s,int} = (8\pi G/5)[(C_{in} - A_{in}) + (C_{o,b} - A_{o,b})] \times [\rho_{sh}(\alpha_{sh} - \alpha_o + \beta_{sh}/2 - \beta_o/2)] (\hat{s}_{sh} \wedge \hat{s}_{in}), \quad (23)$$

where α and β are the polar and equatorial flattenings, defined as the relative differences $((a + b)/2 - c)/(a + b)/2$ and $(a - b)/a$, respectively, with $a > b > c$ the radii in the direction of the principal axes of the layers. For the ocean, we sum the torques on the top and bottom parts

$$\begin{aligned} \vec{\Gamma}_{o,int} &= (8\pi G/5)(C_{in} - A_{in}) [\rho_o(\alpha_o + \beta_o/2)] (\hat{s}_{sh} \wedge \hat{s}_{in}) \\ &\quad - (8\pi G/5)(C_{o,b} - A_{o,b}) \times \\ &\quad [\rho_{sh}(\alpha_{sh} - \alpha_o + \beta_{sh}/2 - \beta_o/2)] (\hat{s}_{sh} \wedge \hat{s}_{in}). \end{aligned} \quad (24)$$

The potential Φ induces a pressure P_{int} in the ocean ($\nabla P_{int} = -\rho_o \nabla \phi$) that modifies the internal gravitational torque on the interior

$$\vec{\Gamma}_{in,int}^p = \int_{V_{in}} (\vec{r} \wedge \rho_o \nabla \Phi) dV. \quad (25)$$

Because of the similarity between Eq.(25) and Eq.(21) and by using Eq.(23), we have

$$\begin{aligned}\vec{\Gamma}_{in,int}^p &= -(8\pi G/5)(C_{o,b} - A_{o,b})[\rho_{sh}(\alpha_{sh} - \alpha_o + \beta_{sh}/2 \\ &\quad - \beta_o/2) + \rho_o(\alpha_o + \beta_o/2)](\hat{s}_{sh} \wedge \hat{s}_{in}).\end{aligned}\quad (26)$$

In the same way as for the interior, we have

$$\begin{aligned}\vec{\Gamma}_{sh,int}^p &= (8\pi G/5)[(C_{in} - A_{in}) + (C_{o,b} - A_{o,b})] \\ &\quad \times [\rho_o(\alpha_o + \beta_o/2)](\hat{s}_{sh} \wedge \hat{s}_{in})\end{aligned}\quad (27)$$

for the shell.

Therefore, $\vec{\Gamma}_{sh,int} + \vec{\Gamma}_{sh,int}^p + \vec{\Gamma}_{in,int} + \vec{\Gamma}_{in,int}^p = 0$. Since the sum of all internal torques must be zero, we have that $\vec{\Gamma}_{o,int} + \vec{\Gamma}_{o,int}^p = 0$ and that the total torque on the ocean is zero. Therefore, we only need to consider the angular momentum equations for the shell and the interior, given by Eqs.(11) and (13). By introducing

$$\kappa'_{sh} = \kappa_{sh} + \kappa_{o,t}, \quad (28)$$

$$\kappa'_{in} = \kappa_{in} + \kappa_{o,b}, \quad (29)$$

$$\begin{aligned}K &= -[(8\pi G)/(5n_T)][(C_{in} - A_{in}) + (C_{o,b} - A_{o,b})] \times \\ &\quad [\rho_{sh}(\alpha_{sh} - \alpha_o + \beta_{sh}/2 - \beta_o/2) + \rho_o(\alpha_o + \beta_o/2)],\end{aligned}\quad (30)$$

the system of angular momentum equation for the shell and the interior, projected onto the Laplace plane, is

$$C_{sh} \frac{dS_{sh}}{dt} = I\kappa'_{sh}(N - S_{sh}) - IK(S_{in} - S_{sh}), \quad (31)$$

$$C_{in} \frac{dS_{in}}{dt} = I\kappa'_{in}(N - S_{in}) + IK(S_{in} - S_{sh}). \quad (32)$$

The two free modes of the system correspond to 'coupled' (with the frequency ω_+) and 'decoupled' (ω_-) modes in which the shell and the interior oscillate in the same and opposite directions, respectively, such that

$$\omega_{\pm} = -(Z \pm \sqrt{\Delta})/(2C_{in}C_{sh}), \quad (33)$$

$$Z = K(C_{in} + C_{sh}) - C_{sh}\kappa'_{in} - C_{in}\kappa'_{sh},$$

$$\Delta = -4C_{in}C_{sh}(-K(\kappa'_{in} + \kappa'_{sh}) + \kappa'_{in}\kappa'_{sh}) + Z^2.$$

For the orbital precession given by Eq.(4), we have, correct up to the first order in inclinations and obliquities, the forced solution for the spin positions

$$S_{sh} = \sum_j (i_j + \varepsilon_{j,sh}) e^{I(\dot{\Omega}_j t + \gamma_j - \pi/2)}, \quad (34)$$

$$S_{in} = \sum_j (i_j + \varepsilon_{j,in}) e^{I(\dot{\Omega}_j t + \gamma_j - \pi/2)}, \quad (35)$$

$$\varepsilon_{j,sh} = \frac{i_j \dot{\Omega}_j (K(C_{sh} + C_{in}) - C_{sh}\kappa'_{in} - C_{in}C_{sh}\dot{\Omega}_j)}{C_{in}C_{sh}(\omega_+ + \dot{\Omega}_j)(\omega_- + \dot{\Omega}_j)}, \quad (36)$$

$$\varepsilon_{j,in} = \frac{i_j \dot{\Omega}_j (K(C_{sh} + C_{in}) - C_{in}\kappa'_{sh} - C_{in}C_{sh}\dot{\Omega}_j)}{C_{in}C_{sh}(\omega_+ + \dot{\Omega}_j)(\omega_- + \dot{\Omega}_j)}. \quad (37)$$

TABLE 2 – **Size and density of the four internal layers of the Titan models consistent with the given constraints on mass and radius** : The ocean thickness and the densities of the core are calculated for the given values of the other interior parameters. Within a given set denoted by curly brackets, the values are equally spaced.

layer	Thickness(km)/Radius(km)	Density (kg m ⁻³)
ice shell	$h_{sh} = \{5\}, \{10, 20, \dots, 200\}$	$\{800, 900, \dots, 1200\}$
ocean	$h_o = 5 - 570$	$\{1000, 1100, \dots, 1400\}$
ice mantle	$R_m = \{2000, 2025, \dots, 2550\}$	$\{1200, 1300, 1400\}$
ice/rock core	$R_c = \{1400, 1410, \dots, 2200\}$	2469 – 3176

For comparisons with the observation, we define the shell obliquity (ε_{sh}), its minimum and maximum values ($\varepsilon_{max,sh}, \varepsilon_{min,sh}$), the deviation (δ_{sh}), and two resonance factors (fr_j^\pm), which describes the amplification of $\varepsilon_{j,sh/in}$ if $\dot{\Omega}_j < 0$ and $\omega_\pm + \Omega_j$ is close to zero, in the same way as for the solid case (Eqs. (7), (8), (9) and (10)).

3.2 Numerical results

The IAU orbit orientation used in [6] is less precise than their determination of the rotation axis orientation and is the main source of error in the obliquity and deviation calculation. By comparing the IAU orbit orientation with those derived from the ephemerides of the JPL HORIZONS system and of the TASS1.6 ([11]), we estimated the obliquity to be $\varepsilon = 0.32 \pm 0.02^\circ$ and the deviation to be $\delta = 0.12 \pm 0.02^\circ$.

We evaluate the solution for a representative range of hydrostatic interior structure models with homogeneous layers of constant density that are constrained by the observed mass and radius (see Table 2). The moments of inertia of the layers depend on the polar and equatorial flattenings due to rotation and static tides that are computed from the Clairaut equation, assuming hydrostatic equilibrium. Among these models, we retain those that have a moment of inertia consistent at the 3σ level with the estimated value of 0.3141 ± 0.0005 of [4].

The periods of the free modes ($T_\pm = 2\pi/\omega_\pm$) and the shell obliquity amplitudes $\varepsilon_{j,sh}$ as a function of the moment of inertia for the interior models are shown in Figs. 1 and 2, respectively. Far from the resonances ($fr_{1,2,4} \simeq 1$), the shell obliquity is below 0.15° . Therefore, a significant resonant amplification of at least one of the $\varepsilon_{j,sh}$ is needed to obtain a time-variable obliquity that can be as large as the observed one ($[\varepsilon_{max,sh}; \varepsilon_{min,sh}] \cap [0.32^\circ - 3\sigma; 0.32^\circ + 3\sigma] \neq \emptyset$). Some interior models have T_+ close to the opposite of the period of Ω_1 or T_- very close to the opposite of the period of $\dot{\Omega}_4$ and have a resonant amplification of $\varepsilon_{1,sh}$ or $\varepsilon_{4,sh}$, respectively, that enables a sufficiently large obliquity value. These interior models are indicated by red and green dots in Figs. 1 and 2, which show that a specific interior model cannot be close to both resonances. Given our range of interior models (see Table 2), some models have the same moment of inertia, but not necessarily the same free mode period, and form vertical lines in Fig. 1. Because of the large number of retained interior models, these vertical lines cannot be easily distinguished, except for those appearing as peaks on the graph of T_+ and corresponding to models with the same h_s, R_c, ρ_m, ρ_o , and ρ_s , such as $\rho_o = \rho_m$, and with different R_m . One can show that T_+ is approximately proportional to C_i for these models and is larger for larger R_m . The interior models at the top of the peaks (red dots), hereafter called class 1 models, are of interest because their shell obliquity can reach the observed value of the obliquity, as a result of a resonant amplification of $\varepsilon_{1,sh}$. These models are characterized by a very large interior

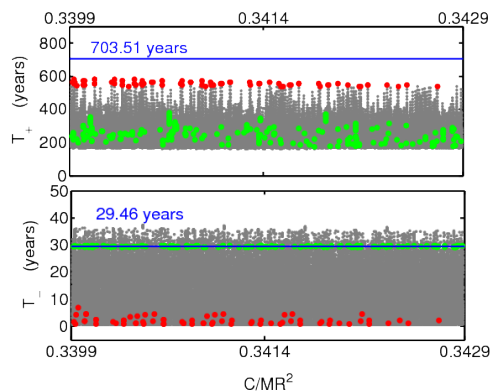


FIGURE 1 – Periods of the ‘coupled’ (T_+) and ‘decoupled’ (T_-) free modes as a function of the moment of inertia, for our range of interior models. The blue horizontal lines represent the opposite of the first and the fourth orbital periods. Some interior models have T_+ close to 703.51 years and other interior models have a period T_- very close to 29.46 years, leading to a resonance. The red and green dots are the interior models that, thanks to a resonant amplification of $\varepsilon_{1,s}$ or $\varepsilon_{4,s}$, can reach a shell obliquity as large as the observed one (see also Fig. 2).

radius of 2525-2550 km, a thin ice shell (5-30 km thickness), and a thin ocean (5-45 km thickness). Interior models that can reach the observed obliquity through a resonant amplification of $\varepsilon_{4,sh}$ (class 2 models) are more diverse than the models of the first class. They are characterized by a thicker ice shell (from 150 to 200 km), an ocean of from 5 to 425 km in thickness, an ice mantle of from 10 to 590 km in thickness and a core radius of between 1800 and 2070 km. Table 3 presents two such resonant models. Model 1 is in resonance with the main period of precession ($fr_1^+ = 5.31 > 1$) and model 2 is in a close resonance with the fourth period of precession ($fr_4^- = 171.11 \gg 1$).

In addition to the obliquity, the deviation of the shell rotation axis from the plane defined by the orbit and Laplace plane normals (see Eq.(9)) has to be consistent with the observations. With a small deviation of 0.03° at best, the class 1 models cannot explain the observed deviation of about 0.12° . The deviation reported by [6] can be seen as an averaged position of the rotation axis during the period of coverage of the analysed radar observations (from Oct 26 2004 to Feb 22 2007), during which model 2 has a deviation smaller than 0.12° . This is true for all the models of class 2 with a positive $\varepsilon_{4,sh}$, because the deviation depends mainly on the ephemerides, particularly on the phases of the orbital precession. We would need to add about 15° and 45° to γ_4 to obtain the correct deviation at time Oct 26 2004 and Feb 22 2007, respectively. However, a comparison of TASS1.6 with a series expansion fitted on the ephemerides of the JPL HORIZONS system convinced us that the phase γ_4 in TASS1.6 is correct up to a few degrees. The series expansion given in [11] is incomplete and additional terms with smaller amplitudes exist (up to $j = 21$, [10]). With those additional terms, some internal models that are consistent with the moment of inertia can account for both the estimated obliquity and deviation, thanks to a combination of a very close resonance between ω_+ and $\hat{\Omega}_{14} = -2\pi/578.73y$, besides the further resonance with $\hat{\Omega}_1$, discussed before. However, this very close resonance seems implausible because of the small fraction of suitable internal structure models.

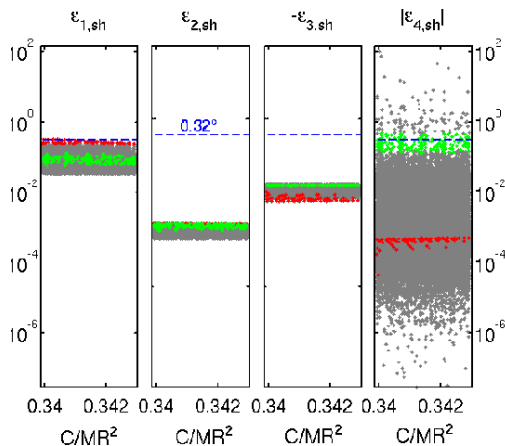


FIGURE 2 – Shell obliquity amplitudes $\varepsilon_{j,sh}$ as a function of the moment of inertia, for our range of interior models. $\varepsilon_{1,sh}$ and $\varepsilon_{2,sh}$ are positive whereas $\varepsilon_{3,sh}$ is negative because of the positive sign of $\dot{\Omega}_3$. $\varepsilon_{4,sh}$ can be either negative or positive since $(\omega_- + \dot{\Omega}_4)$ can be positive or negative. The red/green dots have the same meaning as in Fig. 1.

TABLE 3 – **Internal structure parameters, obliquities, free modes periods, and resonant factors for two resonant models** : Models 1 and 2 are in resonance with the first and the fourth period of precession, respectively.

	Model 1	Model 2
h_{sh}, h_o, R_m, R_c	10, 15, 2550, 1680	170, 105, 2300, 1890
$\rho_{sh}, \rho_o, \rho_m, \rho_c$	1200, 1400, 1400, 3142	1100, 1400, 1400, 2758
$\varepsilon_{1,sh}, \varepsilon_{1,in}$	0.3198 , 1.3816	0.0999, 0.2528
$\varepsilon_{2,sh}, \varepsilon_{2,in}$	0.0007, 0.0032	0.0007, 0.0016
$\varepsilon_{3,sh}, \varepsilon_{3,in}$	-0.0043, -0.0126	-0.0102, -0.0125
$\varepsilon_{4,sh}, \varepsilon_{4,in}$	-0.0004, -0.0023	0.2300 , -0.0270
T_+, T_-	572.019, 2.342	300.391, 29.285
$fr_1^{rig}, fr_2^{rig}, fr_4^{rig}$	5.31 , 1.21, 1.05	1.75, 1.10, 1.11
$fr_1^{dec}, fr_2^{dec}, fr_4^{dec}$	1.00, 1.00, 1.09	1.04, 1.01, 171.11

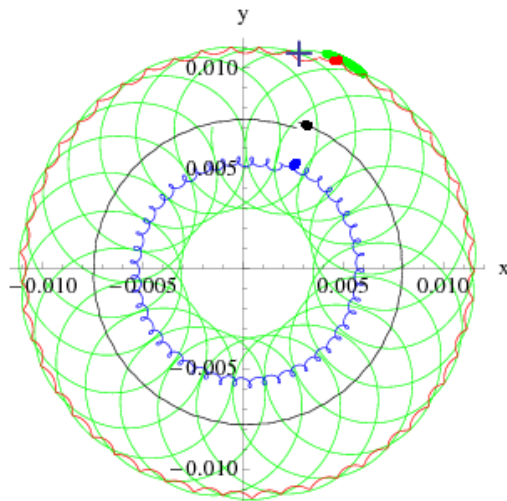


FIGURE 3 – Projection of the normal to the orbit (blue) and of the rotation axis on the Laplace plane (black for the solid case, red for model 1 and green for model 2) over the period of the main precession, beginning at J2000 (thin curves) and over the observation period of [6] (thick curves). The ”+” marker is the projection of the rotation axis measured by [6]. (Unit of the graph is radian.)

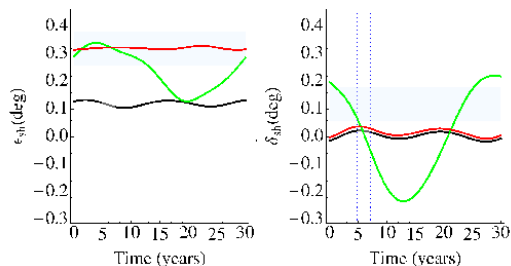


FIGURE 4 – Shell obliquity ε_{sh} (left) and deviation δ_{sh} (right) over 30 years beginning on J2000 (black for the solid case, red for model 1 and green for model 2). The vertical blue lines show the observation period of [6] and the blue boxes represent our estimated obliquity ($0.32^\circ \pm 3\sigma$) and deviation ($0.12^\circ \pm 3\sigma$).

4 Discussion and perspectives

Since we have found a better consistency between the measured and computed positions of the rotation axis with our model than in the solid case, assuming that Titan is locked in the Cassini state, our study is an indication of a possible water ocean layer beneath the surface of Titan.

For two classes of interior models with a liquid water ocean beneath an ice shell, the obliquity computed with our new Cassini state model can be as large as the observed one. However, we rejected the first class of models with a very thin ice shell and a shallow liquid ocean since a thin shell implies high temperatures and therefore, according to the water phase diagram, a thick ocean. On the other hand, models of class 2 are possible but can be quite different so that the estimated obliquity and moment of inertia do not provide accurate constraints on the interior structure.

The theoretically predicted deviation of the rotation axis with respect to the plane defined by the orbit and Laplace plane normals is inconsistent with the observations. We have shown that the use of ephemerides extended to additional frequencies could solve this problem, but only for a small fraction of the rejected class 1 models. Another explanation is that Titan may be slightly offset from the Cassini state because of a recent excitation. However, other explanations extending our Cassini state model might be tested. We have neglected the viscosity at the ocean boundaries because we have assumed that the timescale on which the viscosity is effective is greater than the timescale of the node precession of Titan. We have also neglected the polar motion induced by the atmosphere and the resulting variations in the rotation axis orientation in space since they are expected to have a very small amplitude compared to Titan's obliquity. Although the deformation of the ice shell has not been included, our new Cassini state model is a first step towards a more realistic model of the obliquity of an icy satellite with an ocean.

acknowledgements

R.-M. Baland is a research fellow of the Fonds pour la formation à la Recherche dans l'Industrie et dans l'Agriculture (FRIA), Belgium. This work was financially supported by the Belgian PRODEX program managed by the European Space Agency in collaboration with the Belgian Federal Science Policy Office.

Références

- [1] R.-M. Baland and T. Van Hoolst. Librations of the Galilean satellites : The influence of global internal liquid layers. *Icarus*, 2010.
- [2] B. Bills and F. Nimmo. Spin, gravity, and moments of inertia of Titan. In *European Planetary Science Congress 2009*, pages 553–+, Sept. 2009.
- [3] B. G. Bills. Free and forced obliquities of the Galilean satellites of Jupiter. *Icarus*, 175 :233–247, May 2005.
- [4] L. Iess, N. J. Rappaport, R. A. Jacobson, P. Racioppa, D. J. Stevenson, P. Tortora, J. W. Armstrong, and S. W. Asmar. Gravity Field, Shape, and Moment of Inertia of Titan. *Science*, 327 :1367–, Mar. 2010.
- [5] P. K. Seidelmann, B. A. Archinal, M. F. A'Hearn, D. P. Cruikshank, J. L. Hilton, H. U. Keller, R. J. Oberst, J. L. Simon, P. Stooke, D. J. Tholen, and P. C. Thomas. Working Group on Carto-

- graphic Coordinates and Rotational Elements. *Transactions of the International Astronomical Union, Series A*, 26 :181–181, Mar. 2007.
- [6] B. W. Stiles, R. L. Kirk, R. D. Lorenz, S. Hensley, E. Lee, S. J. Ostro, M. D. Allison, P. S. Callahan, Y. Gim, L. Iess, P. Perci del Marmo, G. Hamilton, W. T. K. Johnson, R. D. West, and The Cassini RADAR Team. Determining Titan’s Spin State from Cassini RADAR Images. *The Astronomical Journal*, 135 :1669–1680, May 2008.
- [7] B. W. Stiles, R. L. Kirk, R. D. Lorenz, S. Hensley, E. Lee, S. J. Ostro, M. D. Allison, P. S. Callahan, Y. Gim, L. Iess, P. Perci del Marmo, G. Hamilton, W. T. K. Johnson, R. D. West, and The Cassini RADAR Team. ERRATUM : ”Determining Titan’s Spin State from Cassini Radar Images” [\[A href=’bib_query\ ?2008AJ....135.1669S’\]\(2008, AJ, 135, 1669\);/A\]. *The Astronomical Journal*, 139 :311–+, Jan. 2010.](#)
- [8] A. M. K. Szeto and S. Xu. Gravitational coupling in a triaxial ellipsoidal Earth. *Journal of Geophysical Research*, 102 :27651–27658, Dec. 1997.
- [9] T. Van Hoolst, N. Rambaux, Ö. Karatekin, and R. Baland. The effect of gravitational and pressure torques on Titan’s length-of-day variations. *Icarus*, 200 :256–264, Mar. 2009.
- [10] A. Vienne. Personal communication. *Personal communication*, 2010.
- [11] A. Vienne and L. Duriez. TASS1.6 : Ephemerides of the major Saturnian satellites. *Astronomy And Astrophysics*, 297 :588–+, May 1995.